Editors' Suggestion | Featured in Physics

Long-Distance Free-Space Measurement-Device-Independent Quantum Key Distribution

Yuan Cao,[1,2,3,*] Yu-Huai Li,[1,2,3,*] Kui-Xing Yang,[1,2,3,*] Yang-Fan Jiang,[1,2,3] Shuang-Lin Li,[1,2,3] Xiao-Long Hu,[4] Maimaiti Abulizi,[1,2,3] Cheng-Long Li,[1,2,3] Weijun Zhang,[5] Qi-Chao Sun,[1,2,3] Wei-Yue Liu,[1,2,3] Xiao Jiang,[1,2,3] Sheng-Kai Liao,[1,2,3] Ji-Gang Ren,[1,2,3] Hao Li,[5] Lixing You,[5] Zhen Wang,[5] Juan Yin,[1,2,3] Chao-Yang Lu,[1,2,3] Xiang-Bin Wang,[2,4,†] Qiang Zhang,[1,2,3,‡] Cheng-Zhi Peng,[1,2,3,§] and Jian-Wei Pan[1,2,3,‖]

[1]*Hefei National Laboratory for Physical Sciences at the Microscale and Department of Modern Physics, University of Science and Technology of China, Hefei 230026, China*

[2]*Shanghai Branch, CAS Center for Excellence in Quantum Information and Quantum Physics, University of Science and Technology of China, Shanghai 201315, China*

[3]*Shanghai Research Center for Quantum Sciences, Shanghai 201315, China*

[4]*State Key Laboratory of Low Dimensional Quantum Physics, Tsinghua University, Beijing 100084, People's Republic of China*

[5]*State Key Laboratory of Functional Materials for Informatics, Shanghai Institute of Microsystem and Information Technology, Chinese Academy of Sciences, Shanghai 200050, People's Republic of China*

(Received 7 June 2020; accepted 11 November 2020; published 23 December 2020)

Measurement-device-independent quantum key distribution (MDI-QKD), based on two-photon interference, is immune to all attacks against the detection system and allows a QKD network with untrusted relays. Since the MDI-QKD protocol was proposed, fiber-based implementations aimed at longer distance, higher key rates, and network verification have been rapidly developed. However, owing to the effect of atmospheric turbulence, MDI-QKD over a free-space channel remains experimentally challenging. Herein, by developing a robust adaptive optics system, high-precision time synchronization and frequency locking between independent photon sources located far apart, we realized the first free-space MDI-QKD over a 19.2-km urban atmospheric channel, which well exceeds the effective atmospheric thickness. Our experiment takes the first step toward satellite-based MDI-QKD. Moreover, the technology developed herein opens the way to quantum experiments in free space involving long-distance interference of independent single photons.

DOI: 10.1103/PhysRevLett.125.260503

A series of interesting experiments based on the *Micius* satellite have been performed aimed at global-scale quantum communications [1–6], including satellite-based quantum key distribution (QKD) with decoy-state BB84 [1,2,7–9] and entanglement-based [4,6,10,11] protocol. Naturally, the next step is to realize satellite-based measurement-device-independent (MDI) QKD [12,13], which is immune to any attack against the detection. Combined with the decoy-state method [8,9], which closes the most critical loophole in the source, the MDI proposal has greatly improved the security of realistic systems [14].

Although several MDI-QKD experiments have been performed [15–22] over optical fiber, none of them have been implemented with a free-space channel. The main reason is that the amplitude and phase fluctuation induced by atmospheric turbulence makes it difficult to maintain the indistinguishability in terms of spatial, timing, and spectral modes between independent photons. Therefore, fiber-based MDI-QKD technology could not be directly adopted in free-space links. Here, by developing new techniques of adaptive optics (AO), remote synchronization and frequency locking, we demonstrate the first MDI-QKD over a two-link noisy free-space channel from two sites in Shanghai, separated by approximately 20 km, as shown in Fig. 1(a).

Atmospheric turbulence inevitably affects the wave front of laser beams and results in the varying random distribution of amplitude and phase at the receiving aperture. The strength of the turbulence is usually described by the Fried parameter r_0 [23] or Fried's coherence length. When using receiver telescopes with a diameter D_r considerably larger than r_0 (typically ~0.5–5 cm for a 10-km terrestrial free-space channel), the direct interference with two laser pulses propagated through different atmospheric channels suffers from spatial mode distinguishability [24,25]. This can be solved by applying a spatial mode filter, such as single mode fibers (SMFs). This, however, results in additional coupling loss, which is typically approximately 2 orders of magnitude higher than that using multimode fibers. Therefore, the first challenge is to couple arriving photons into SMFs with acceptable efficiency.

AO is widely used in astronomical observation with large-diameter telescopes, where the effect of atmospheric turbulence is the main bottleneck in further increasing the resolution. However, the application of AO in a horizontal

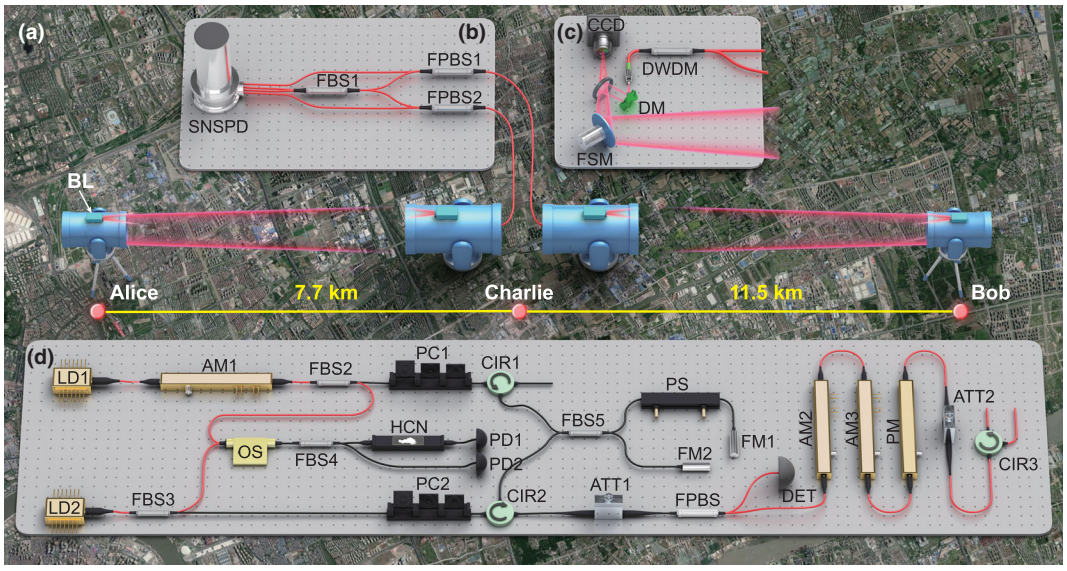

FIG. 1. Setup of free-space MDI-QKD. (a) Top view of the experimental layout at the Pudong area, Shanghai. Alice and Bob are in opposite directions from the measurement station, at distances of 7.7 and 11.5 km, respectively. (b) Arriving photon pulses interference on a fiber beam splitter (FBS) are detected by superconducting nanowire single photon detectors (SNSPDs). Before entering the FBS, a fiber polarization beam splitter (FPBS) is employed to filter the polarization, allowing about 10% to be directly measured for time synchronization. (c) A camera and a fast steering mirror (FSM) together operate as the acquiring, pointing, and tracking system. The stochastic parallel gradient descent algorithm-based AO system compensates the wave front aberration to maximize the coupling efficiency of SMFs using a DM. (d) The photon sources for MDI-QKD at Alice and Bob. A hydrogen cyanide (HCN) molecule absorption cell is employed to calibrate the wavelength of two DFB laser diodes (LDs). The optical pulses generated from LD1 are further modulated by an amplitude modulator (AM) to obtain better uniformity. An asymmetric interferometer is employed to generate pulse pairs. To ensure the relative phase between the two pulses, the interferometer is phase locked by continuous wave laser emitted from LD2 at the same wavelength as that of the signal laser. The encoding is performed by two AMs and a phase modulator (PM). Note: OS, optical switch; CIR, circulator; FM, Faraday mirror; PC, polarization controller; PS, phase shifter; PD, photodiode; DET, single photon detector; BL, beacon laser; DWDM, dense wavelength division multiplexing; ATT, attenuation.

free-space channel remains uncommon. An important reason for this is that the turbulence of the horizontal atmosphere in a common environment (e.g., urban area) is much stronger than that in the vertical atmosphere with good seeing; this issue is challenging for the AO system. In general, the AO system comprises a wave front sensor and a wave front compensator. The Shack-Hartmann detector is a good wave front sensor that can directly estimate the wave front with a high sampling frequency. Moreover, micro-electromechanical-system- or piezoelectric-based deformable mirrors (DMs) are common wave front compensators that contain a large number of independent units. However, under strong turbulence, it is difficult to effectively estimate wave front owing to intensity scintillations and phase singularities [26,27]. Therefore, an AO system without wave front sensors is desired [28]. Herein, we employed a stochastic parallel gradient descent algorithm-based method to perform wave front aberration correction (see Supplemental Material [29]). A 1570-nm laser was employed, which was transmitted through the same path with the signal photons, to probe the efficiency of the free-space channel as the input of the AO system. With a close-loop bandwidth of 1 kHz, we operated the AO system to compensate the first 12 orders of Zernike aberration and obtained an improvement in the SMF coupling efficiency by an average of 3–6 dB, which indicates a total improvement of 6–12 dB for two free-space channels.

In addition to the spatial mode matching, the timing and frequency modes also require special attention. To achieve high visibility, the time duration Δt and frequency spread $\Delta\nu$ of interfering photon pulses are required to approach the limitation of the uncertainty principle $\Delta t\Delta\nu \sim 1/4\pi$ [32]. Thus, the time synchronization accuracy $\delta t \ll \Delta t$ and the frequency difference $\delta\nu \ll \Delta\nu$ should satisfy $\delta t\delta\nu \ll 1/4\pi$. In most previous fiber-based experiments that used the interference of two independent photon sources, including MDI-QKD [17] and twin-field QKD [33], a master clock was shared between these two sources, either by electronic cables or fibers, and strong optical pulses were shared to compare or calibrate frequencies. However, in the free-space channel, the transmitted optical signals may be disturbed by turbulence, which results in a considerable intensity fluctuation. Therefore, sharing the time and frequency via free-space links is very challenging. Here, we employed independent ultrastable crystal oscillators as clocks for each photon source and measurement station (see Supplemental Material [29]). A portion of the arriving photons is directly measured in the SNSPDs to estimate the

time and frequency difference between the oscillators as the input of feedback control. By tuning the delay and frequency of the clocks accordingly, the measured standard deviation of the arrival time difference between optical pulses from two sources δt was 32 ps.

Previous fiber systems would routinely send strong laser signals to an optical spectrum analyzer at the middle station to measure and feed back the spectrum. However, in the free-space channel, the transmitted optical signal intensity would fluctuate, which would ruin the spectrum measurement. Herein, we employed two independent hydrogen cyanide molecule cells as the frequency standard in two sending stations. As shown in Fig. 1(d), laser power is measured before and after the molecule cell by photodiodes to calculate the absorption rate. With proper temperature control and stable driving current, the wavelengths of the distributed feedback (DFB) LDs were calibrated to 1550.52 nm, with a difference $\delta\nu$ of at most 10 MHz between two independent diodes. Finally, appropriate time synchronization and frequency calibration $\delta t\delta\nu \sim 3 \times 10^{-4} \ll 1/4\pi$ enables a large range of selectable Δt and $\Delta\nu$.

An advantage of using a free-space channel is that maintaining the polarization is much easier than in a fiber. The polarization state can have high fidelity even after propagation through a near-ground atmosphere on the order of 100 km [34,35] or a satellite-to-ground link over 1000 km [1]. Herein, we employed a fiber polarizing beam splitter to ensure the indistinguishability of polarization before interference, as shown in Fig. 1(b). By tuning the related fiber polarization controller, approximately 90% of the arriving photons entered the fiber beam splitter for interference, while the remaining photons were directly measured for the feedback of time synchronization.

Furthermore, a demonstration of the asymmetric four-intensity decoy-state MDI-QKD protocol [36,37] was implemented with time-bin qubits. In the Z basis, the key bit is encoded in time-bin 0 or time-bin 1, on the amplitude modulator AM2 and AM3. In the X basis, the key bit is encoded into the linear superposition state with relative phases 0 or π between the two time bins by a PM. The four-intensity scheme [36] was adopted where each side of Alice and Bob use four different intensities: Alice (Bob) use signal state of intensity $\mu_{z(a)}$ ($\mu_{z(b)}$) in the Z basis, decoy states of intensity $\mu_{x_1(a)}, \mu_{x_2(a)}$ ($\mu_{x_1(b)}, \mu_{x_2(b)}$) in the X basis (X_1 or X_2), and vacuum state O (see Supplemental Material [29]). As shown in Fig. 1(a), two photon sources are separated by 19.2 km. The measurement station is placed between them, with distances of 7.7 and 11.5 km, respectively. In each photon source, an arbitrary waveform generator, which is locked on the crystal oscillator, is employed to produce electronic signals for LDs and modulators. The details of the photon source are shown in Fig. 1(d). The optical pulses generated from the DFB LDs, which had a repetition rate of 100 MHz and width of 2 ns, were further modulated on AM1 to obtain better uniformity and encode decoy states. An asymmetric Mach-Zehnder (MZ) interferometer was employed to generate coherent pulse pairs that were separated by $\Delta T = 3$ ns. The asymmetric MZ interferometer is required to be phase locked to ensure that the X basis has the same reference frame between different photon sources. Phase difference was estimated by measuring the probability of photons exiting a certain port of the interferometer with an additional continuous wave (cw) laser, as shown in Fig. 1(d). To reduce cross talk between the pulsed signal laser and cw phase-locking laser, polarization and temporal filtering were employed (see Supplemental Material [29]). The frequency of the reference cw laser was calibrated using the same molecule absorption cell to ensure that the frequency difference between the cw laser and signal laser $\Delta\nu_r$ remains below 10 MHz. Thus, the accuracy of the estimated phase by the reference cw laser is expected to be better than $2\pi\Delta\nu_r\Delta T \sim 0.19$ rad. Several intensity modulators and a PM were employed to perform the encoding.

Hong–Ou–Mandel (HOM) interference with a visibility of 0.412 ± 0.001 was directly observed on the coincidence count between two SNSPDs channels, as shown in Fig. 2. The imperfection of visibility is mainly owing to the intensity mismatch caused by the atmospheric turbulence. Together with a fast photodiode, the reference laser for AO can give a good indication for estimating the varying efficiency of free-space channels. The reference laser powers of every time slot (set as 1 ms) are recorded to perform data postselection to increase the indistinguishability of the interfering pulses. For each time slot, the intensity ratio for corresponding pulses is estimated by $r_p = \min(P_1, P_2)/\max(P_1, P_2)$, where P_1 and P_2 are the

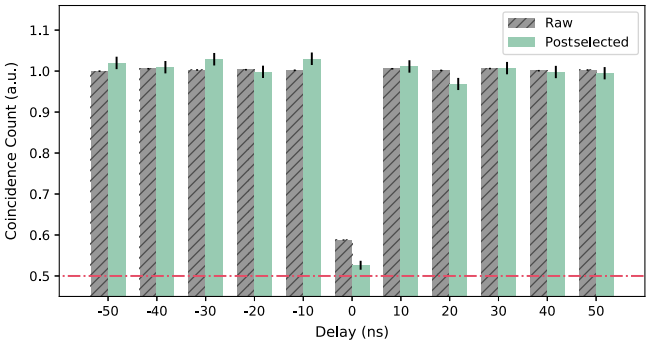

FIG. 2. Coincidence count of the HOM interference over a long-distance free-space channel. By scanning the time delay of the two detector channels, the coincidence count varies to show the visibility. With all data counted in, the visibility is 0.412 ± 0.001, which is mainly effected by the fluctuation of channel efficiency. Further data postselecting occurs with the assistance of an additional reference laser. By ruling out pulse pairs with a different average photon number (by the threshold of 0.98), a visibility of 0.474 ± 0.010 is obtained, which is close to the limitation of HOM interference by coherence states.

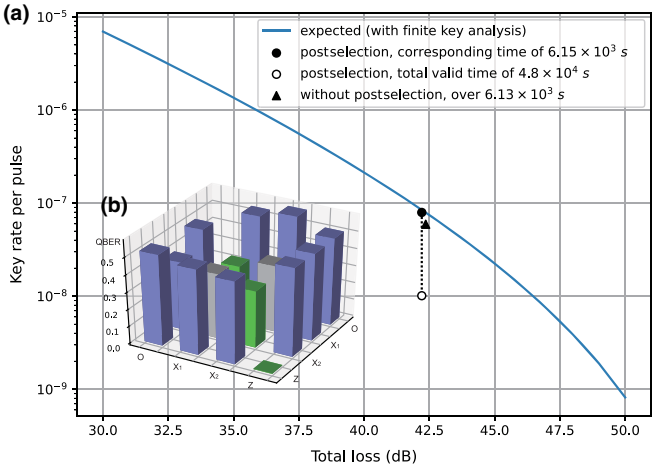

FIG. 3. Results of MDI-QKD. (a) With the postselection process, 6.15×10^3 s of valid time are selected from entire data of 4.8×10^4 s using a threshold of $r_p > 0.8$. The final key rate per pulse of 7.94×10^{-8} (consideration finite key length) is shown as the solid circle, which is close to the simulated curve. The hollow circle represents the effective secure key rate of postselected data over entire data taking duration, i.e., 4.8×10^4 s, which is diminished significantly to 1.01×10^{-8}. The secure key rate without postselection is calculated as 5.93×10^{-8} by data over 6.13×10^3 s, shown as the triangle. For a fair comparison, these time slots comprising four sets of continuously acquired data picked from the entire dataset have total loss and valid time similar to those of the postselected data. (b) Quantum bit error rates for each basis. QBERs for the Z-Z and X_1-X_1 bases are 0.23% and 33.6%, respectively.

powers of the reference lasers. With a proper threshold to discard mismatched pulses, the visibility of HOM interference can be increased to 0.474 ± 0.010. With a set of optimized parameters, as shown in Table I, more than 3.5×10^6 sifted keys in the Z-Z basis were obtained in 13.4 h. The quantum bit error rates (QBERs) for each basis are shown in Fig. 3(b). Particularly, QBERs for the Z-Z and X_1-X_1 bases were 0.23% and 33.6%, respectively. With the consideration of finite key length, over 295 kbit of secure keys were generated, which corresponded to a key rate of 6.11 bps. As can be speculated from the results of HOM interference, postselection effectively reduces QBER for the X_1-X_1 basis down to 29.8%, thereby improving the secure key rate over corresponding time. The secure key rates with and without postselection are compared in Fig. 3(a). Depending on the condition of the channel, e.g., the average loss and strength of atmospheric turbulence, the total number of secure keys after postselection might diminish owing to the reduction in corresponding time. However, under violent atmospheric turbulence, postselection could be a necessary method for obtaining a positive final key rate.

In this Letter, we experimentally demonstrated a 19.2-km free-space MDI-QKD with asymmetric, unstable channels. The distance achieved in this experiment is well beyond the effective thickness of the aerosphere (~10 km), and the turbulence of the horizontal atmospheric channel is normally much stronger than that of the vertical channel. Moreover, we demonstrated time and frequency synchronization between independent terminals without a stable channel. Thus, we have presented a significant step toward satellite-based MDI-QKD. Indeed, satellite-based MDI-QKD is an ambitious goal facing many technique challenges, including high loss, atmospheric fluctuation, satellite motion, time and frequency synchronization between independent terminals, and spaceborne single photon detectors [38], among others. Overcoming these technical challenges will be the next goal for us. In addition to the final goal of satellite-based MDI-QKD, it is worth noting that the horizontal free-space channel is an important reinforcement for the fiber-based channel owing to its configurational flexibility.

The technique developed is also suitable for a fiber-based MDI-QKD system. In this case, no extra fiber channels are required for the transmission of classical analog signals such as clock and optical frequency reference. Therefore, the structure of the MDI-QKD network in free space and fiber can be considerably simplified. The setup is naturally suitable for the daylight QKD [39,40] benefit from the single mode fiber coupling. In the future, a higher clock rate, and thus a higher key rate, can be obtained by improving the accuracy of time synchronization. It is worth noting that, for shorter

TABLE I. Device parameters for the optimization of the asymmetric four-intensity decoy-state method [36,37] for MDI-QKD: dark count rate d_0, misalignment error probabilities of the Z basis E_a^Z and X_1 basis $E_a^{X_1}$, channel efficiency between Alice (Bob) and Charlie η_A (η_B), efficiency of the measurement module at Charlie η_M, error-correction efficiency f, failure probability in the statistical fluctuation analysis of one observable ϵ, and total number of pulse pairs N. The security coefficient of the whole protocol is $\epsilon_{\text{total}} = 16\epsilon = 1.6 \times 10^{-6}$. The optimized source parameters are listed in the lower part of the table.

d_0	E_a^Z	$E_a^{X_1}$	η_A	η_B	η_M	f	ϵ	N
7×10^{-7}	0.3%	3%	17 dB	20 dB	3 dB	1.10	10^{-7}	10^{12}
		μ_{x_1}	μ_{x_2}	μ_z	p_o	p_{x_1}	p_{x_2}	p_z
Alice		0.0394	0.155	0.335	0.0327	0.383	0.0863	0.498
Bob		0.0713	0.280	0.488	0.0291	0.381	0.0859	0.504

pulses, the frequency span will be broadened, thereby reducing the requirement of optical frequency calibration. The MDI-QKD can be further extended to the case of high-dimensional encoding [41], which is also an approach for increasing the key rate. In addition, with the help of integrated photonics [42], it is possible to develop a compact source with low cost and low-power dissipation which is suitable for being deployed on the CubeSat. Furthermore, the two-photon interference in long-distance free-space channels realized in this Letter can be applied directly in various other quantum information processing, such as twin-field QKD [43], quantum teleportation [44], quantum repeaters [45], and quantum networks [46].

We acknowledge insightful discussions with Teng-Yun Chen, Hao Liang, Fu-Tian Liang, and Li-Hua Sun. This work was supported by the National Key R&D Program of China (Grants No. 2017YFA0303900 and No. 2017YFA0304000), the National Natural Science Foundation of China (Grants No. U1738201, No. U1738142, No. 11654005, No. 11904358, No. 61625503, No. 11822409, and No. 11674309), the Chinese Academy of Sciences (CAS), Shanghai Municipal Science and Technology Major Project (Grant No. 2019SHZDZX01), and Anhui Initiative in Quantum Information Technologies. Y. C. was supported by the Youth Innovation Promotion Association of CAS (under Grant No. 2018492).

*These authors contributed equally to this work.
†xbwang@mail.tsinghua.edu.cn
‡qiangzh@ustc.edu.cn
§pcz@ustc.edu.cn
‖pan@ustc.edu.cn

[1] S.-K. Liao *et al.*, Nature (London) **549**, 43 (2017).
[2] S.-K. Liao *et al.*, Phys. Rev. Lett. **120**, 030501 (2018).
[3] J. Yin *et al.*, Science **356**, 1140 (2017).
[4] J. Yin, Y. Cao, Y.-H. Li, J.-G. Ren, S.-K. Liao, L. Zhang, W.-Q. Cai, W.-Y. Liu, B. Li, H. Dai, M. Li, Y.-M. Huang, L. Deng, L. Li, Q. Zhang, N.-L. Liu, Y.-A. Chen, C.-Y. Lu, R. Shu, C.-Z. Peng, J.-Y. Wang, and J.-W. Pan, Phys. Rev. Lett. **119**, 200501 (2017).
[5] J.-G. Ren *et al.*, Nature (London) **549**, 70 (2017).
[6] J. Yin, Y. H. Li, S. K. Liao, M. Yang, Y. Cao, L. Zhang, J. G. Ren, W. Q. Cai, W. Y. Liu, S. L. Li, R. Shu, Y. M. Huang, L. Deng, L. Li, Q. Zhang, N. L. Liu, Y. A. Chen, C. Y. Lu, X. B. Wang, F. Xu, J. Y. Wang, C. Z. Peng, A. K. Ekert, and J. W. Pan, Nature (London) **582**, 501 (2020).
[7] C. H. Bennett and G. Brassard, in *Proceedings of the IEEE International Conference on Computers, Systems and Signal Processing* (IEEE Press, New York, 1984), pp. 175–179.
[8] X.-B. Wang, Phys. Rev. Lett. **94**, 230503 (2005).
[9] H.-K. Lo, X. Ma, and K. Chen, Phys. Rev. Lett. **94**, 230504 (2005).
[10] C. H. Bennett, G. Brassard, and N. D. Mermin, Phys. Rev. Lett. **68**, 557 (1992).
[11] A. K. Ekert, Phys. Rev. Lett. **67**, 661 (1991).
[12] H.-K. Lo, M. Curty, and B. Qi, Phys. Rev. Lett. **108**, 130503 (2012).
[13] S. L. Braunstein and S. Pirandola, Phys. Rev. Lett. **108**, 130502 (2012).
[14] F. Xu, X. Ma, Q. Zhang, H.-K. Lo, and J.-W. Pan, Rev. Mod. Phys. **92**, 025002 (2020).
[15] Y. Liu, T.-Y. Chen, L.-J. Wang, H. Liang, G.-L. Shentu, J. Wang, K. Cui, H.-L. Yin, N.-L. Liu, L. Li, X. Ma, J. S. Pelc, M. M. Fejer, C.-Z. Peng, Q. Zhang, and J.-W. Pan, Phys. Rev. Lett. **111**, 130502 (2013).
[16] A. Rubenok, J. A. Slater, P. Chan, I. Lucio-Martinez, and W. Tittel, Phys. Rev. Lett. **111**, 130501 (2013).
[17] Y.-L. Tang, H.-L. Yin, S.-J. Chen, Y. Liu, W.-J. Zhang, X. Jiang, L. Zhang, J. Wang, L.-X. You, J.-Y. Guan, D.-X. Yang, Z. Wang, H. Liang, Z. Zhang, N. Zhou, X. Ma, T.-Y. Chen, Q. Zhang, and J.-W. Pan, Phys. Rev. Lett. **113**, 190501 (2014).
[18] H.-L. Yin, T.-Y. Chen, Z.-W. Yu, H. Liu, L.-X. You, Y.-H. Zhou, S.-J. Chen, Y. Mao, M.-Q. Huang, W.-J. Zhang, H. Chen, M. J. Li, D. Nolan, F. Zhou, X. Jiang, Z. Wang, Q. Zhang, X.-B. Wang, and J.-W. Pan, Phys. Rev. Lett. **117**, 190501 (2016).
[19] S. Pirandola, C. Ottaviani, G. Spedalieri, C. Weedbrook, S. L. Braunstein, S. Lloyd, T. Gehring, C. S. Jacobsen, and U. L. Andersen, Nat. Photonics **9**, 397 (2015).
[20] L. C. Comandar, M. Lucamarini, B. Fröhlich, J. F. Dynes, A. W. Sharpe, S. W.-B. Tam, Z. L. Yuan, R. V. Penty, and A. J. Shields, Nat. Photonics **10**, 312 (2016).
[21] Y.-L. Tang, H.-L. Yin, Q. Zhao, H. Liu, X.-X. Sun, M.-Q. Huang, W.-J. Zhang, S.-J. Chen, L. Zhang, L.-X. You, Z. Wang, Y. Liu, C.-Y. Lu, X. Jiang, X. Ma, Q. Zhang, T.-Y. Chen, and J.-W. Pan, Phys. Rev. X **6**, 011024 (2016).
[22] H. Liu, W. Wang, K. Wei, X.-T. Fang, L. Li, N.-L. Liu, H. Liang, S.-J. Zhang, W. Zhang, H. Li, L. You, Z. Wang, H.-K. Lo, T.-Y. Chen, F. Xu, and J.-W. Pan, Phys. Rev. Lett. **122**, 160501 (2019).
[23] D. L. Fried, J. Opt. Soc. Am. **56**, 1372 (1966).
[24] L. C. Andrews and R. L. Phillips, *Laser Beam Propagation through Random Media*, 2nd ed. (SPIE, Bellingham, 2005).
[25] W. C. Swann, L. C. Sinclair, I. Khader, H. Bergeron, J.-D. Deschênes, and N. R. Newbury, Appl. Opt. **56**, 9406 (2017).
[26] J. D. Barchers, D. L. Fried, and D. J. Link, Appl. Opt. **41**, 1012 (2002).
[27] D. L. Fried, J. Opt. Soc. Am. A **15**, 2759 (1998).
[28] M. A. Vorontsov, G. W. Carhart, and J. C. Ricklin, Opt. Lett. **22**, 907 (1997).
[29] See Supplemental Material at http://link.aps.org/supplemental/10.1103/PhysRevLett.125.260503 for a detailed description of adaptive optics, time synchronization, and asymmetric four-intensity decoy-state MDI-QKD, which includes Refs. [30,31].
[30] Z.-W. Yu, Y.-H. Zhou, and X.-B. Wang, Phys. Rev. A **91**, 032318 (2015).
[31] X.-B. Wang, Phys. Rev. A **87**, 012320 (2013).
[32] P. Pfeifer and J. Fröhlich, Rev. Mod. Phys. **67**, 759 (1995).
[33] Y. Liu, Z.-W. Yu, W. Zhang, J.-Y. Guan, J.-P. Chen, C. Zhang, X.-L. Hu, H. Li, C. Jiang, J. Lin, T.-Y. Chen, L. You, Z. Wang, X.-B. Wang, Q. Zhang, and J.-W. Pan, Phys. Rev. Lett. **123**, 100505 (2019).

[34] J. Yin, J.-G. Ren, H. Lu, Y. Cao, H.-L. Yong, Y.-P. Wu, C. Liu, S.-K. Liao, F. Zhou, Y. Jiang, X.-D. Cai, P. Xu, G.-S. Pan, J.-J. Jia, Y.-M. Huang, H. Yin, J.-Y. Wang, Y.-A. Chen, C.-Z. Peng, and J.-W. Pan, Nature (London) **488**, 185 (2012).
[35] X.-S. Ma, T. Herbst, T. Scheidl, D. Wang, S. Kropatschek, W. Naylor, B. Wittmann, A. Mech, J. Kofler, E. Anisimova, V. Makarov, T. Jennewein, R. Ursin, and A. Zeilinger, Nature (London) **489**, 269 (2012).
[36] Y.-H. Zhou, Z.-W. Yu, and X.-B. Wang, Phys. Rev. A **93**, 042324 (2016).
[37] X.-L. Hu, Y. Cao, Z.-W. Yu, and X.-B. Wang, Sci. Rep. **8**, 17634 (2018).
[38] L. You, J. Quan, Y. Wang, Y. Ma, X. Yang, Y. Liu, H. Li, J. Li, J. Wang, J. Liang, Z. Wang, and X. Xie, Opt. Express **26**, 2965 (2018).
[39] S.-K. Liao *et al.*, Nat. Photonics **11**, 509 (2017).
[40] M. Avesani, L. Calderaro, M. Schiavon, A. Stanco, C. Agnesi, A. Santamato, M. Zahidy, A. Scriminich, G. Foletto, G. Contestabile, M. Chiesa, D. Rotta, M. Artiglia, A. Montanaro, M. Romagnoli, V. Sorianello, F. Vedovato, G. Vallone, and P. Villoresi, arXiv:1907.10039.
[41] L. Dellantonio, A. S. Sørensen, and D. Bacco, Phys. Rev. A **98**, 062301 (2018).
[42] K. Wei, W. Li, H. Tan, Y. Li, H. Min, W.-J. Zhang, H. Li, L. You, Z. Wang, X. Jiang, T.-Y. Chen, S.-K. Liao, C.-Z. Peng, F. Xu, and J.-W. Pan, Phys. Rev. X **10**, 031030 (2020).
[43] M. Lucamarini, Z. L. Yuan, J. F. Dynes, and S. A. J., Nature (London) **557**, 400 (2018).
[44] C. H. Bennett, G. Brassard, C. Crepeau, R. Jozsa, A. Peres, and W. K. Wootters, Phys. Rev. Lett. **70**, 1895 (1993).
[45] H.-J. Briegel, W. Dür, J. I. Cirac, and P. Zoller, Phys. Rev. Lett. **81**, 5932 (1998).
[46] M. Halder, A. Beveratos, N. Gisin, V. Scarani, and H. Zbinden, Nat. Phys. **3**, 692 (2007).